Letter

Trapping and binding by dephasing

K. Mukherjee, S. Poddar, and S. Wüster*

Department of Physics, Indian Institute of Science Education and Research, Bhopal, Madhya Pradesh 462 066, India

(Received 27 September 2021; accepted 11 April 2022; published 22 April 2022)

The binding and trapping of particles usually rely on conservative forces, described by unitary quantum dynamics. We show that both can also arise solely from spatially dependent dephasing, the simplest type of decoherence. This can be based on continuous weak position measurements in only selected regions of space, for which we propose a practical realization. For a single particle, we demonstrate a quantum particle in a box based on dephasing. For two particles, we demonstrate their binding despite repulsive interactions, if their molecular states are dephased at large separations only. Both mechanisms are experimentally accessible, as we show for an example with Rydberg atoms in a cold gas background.

DOI: 10.1103/PhysRevA.105.L041102

Introduction. Bound states due to conservative forces are central to our existence, combining fundamental particles into atoms, those into molecules, and the latter into complex biological structures. Many binding mechanisms arise from emergent rather than fundamental forces, and can be very weak, even while essential, such as when Cooper pairs bound by lattice-phonon mediated interactions cause superconductivity. Quantum coherence is often a crucial element of the bound state, as in the molecular states of the H_2^+ molecule, which change character from covalent binding to repelling depending on the relative phase of atomic orbitals [1]. In larger systems, decoherence can become relevant [2,3], and while usually detrimental for quantum technologies [4], it can also be a resource [5–7].

Trapping and binding are two key requirements for complexity, and we show here that both can also arise due to the simplest type of decoherence: dephasing. Trapping in our proposal exploits the quantum Zeno effect [8,9], as the position of a particle is inferred only *outside* the trapping region [10–13], and similarly binding relies on relative distance measurements that are only sensitive to large distances.

This enables a further class of decoherence processes, namely pure dephasing, as a tool for the incoherent quantum state engineering [6] of trapped states or bound states for quantum technologies. The emergence of such states was earlier shown only due to decoherence arising from loss processes and therefore involving dissipation as well [7,10,14–19], which is not important here.

To begin, we summarize how the spatially selective position and internal state measurement of particles can affect their motion, described by an effective master equation. To be specific we discuss the examples of a single Rydberg atom and a Rydberg dimer, for which a surrounding ultracold gas can provide the required position and state quantum nondemolition (QND) measurement (see Fig. 1), but the principles can be ported to other platforms. Next, we construct an equivalent of the well-known particle in a box, but based on dephasing. In the final two sections we reach our main result, generalizing single-particle trapping to a two-particle bound state.

Spatially selective dephasing. We first outline a general theory of N Rydberg atoms embedded in an ultracold gas, which we later apply to a single Rydberg atom ($N = 1$) or a Rydberg dimer ($N = 2$), as sketched in Fig. 1. We let each Rydberg atom to be in states $|s\rangle = |\nu s\rangle$ and $|p\rangle = |\nu p\rangle$ with a high principal quantum number ν. The system can thus be in electronic states $|\pi_n\rangle = |ss\cdots p\cdots s\rangle$, where the nth atom is in $|p\rangle$ and the rest are in $|s\rangle$ [20]. The effective Hilbert space for the surrounding cold gas atoms is $\{|g\rangle, |e\rangle, |u\rangle\}$, predominantly in the electronic ground state $|g\rangle$, but optically coupled via a low-lying excited state $|e\rangle$ to an auxiliary Rydberg excited

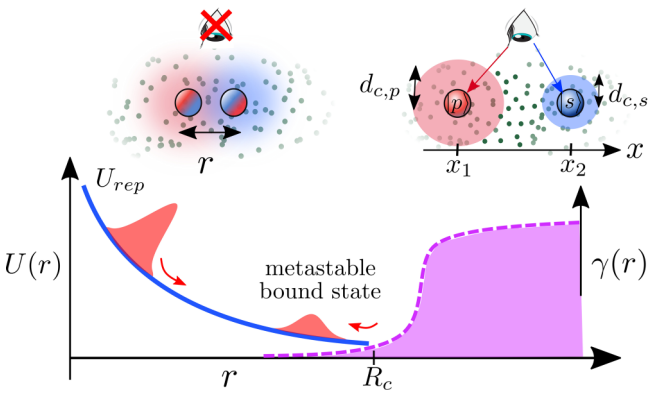

FIG. 1. Selective relative distance measurements. A dimer of Rydberg atoms in $|s\rangle$ and $|p\rangle$ states (blue and red spheres) is separated by a distance r and immersed in an ambient medium of ground-state atoms (green). Top: Electromagnetically induced transparency (EIT) in the medium can be used to measure the position x and state of dimer atoms at large separation (top right) $r = |x_2 - x_1|$, whereas this breaks down at small r (top left). Bottom: The nuclear wave function of the dimer (red) on a repulsive potential $U_{\rm rep}(r)$ (blue) can then reflect off the steep dephasing profile $\gamma(r)$ (violet dashed) at large separation ($r \sim R_c$), forming a metastable bound state.

*sebastian@iiserb.ac.in

state $|u\rangle = |\nu' s\rangle$, $\nu' \neq \nu$, in a ladder configuration resulting in Rydberg electromagnetically induced transparency (EIT) [21–28]. In this configuration the cold gas atoms only occupy the $|u\rangle$ state with a very low probability, hence we do not refer to them as Rydberg atoms, but as background atoms. We group all positions $\mathbf{X}_n$ of Rydberg atoms with latin indices n into a collective coordinate $\mathbf{X} = [\mathbf{X}_1, \mathbf{X}_2, \ldots, \mathbf{X}_N]^T$ and similarly for background atoms $\mathbf{x} = [\mathbf{x}_1, \ldots, \mathbf{x}_{N_{\rm bg}}]^T$ at position $\mathbf{x}_\alpha$, using greek indices for those.

The starting point for modeling is the many-body master equation

$$\dot{\hat{\rho}} = -i[\hat{H}, \hat{\rho}] + \sum_\alpha \mathcal{L}_{\hat{L}_\alpha}[\hat{\rho}], \tag{1}$$

where $\hat{H}$ is the total Hamiltonian, $\hat{\rho}$ the density matrix, and $\mathcal{L}_{\hat{L}_\alpha}$ a superoperator $\mathcal{L}_{\hat{O}} = \hat{O}\hat{\rho}\hat{O}^\dagger - (\hat{O}^\dagger\hat{O}\hat{\rho} + \hat{\rho}\hat{O}^\dagger\hat{O})/2$, for spontaneous decay from $|e\rangle$ to $|g\rangle$ via the decay operator $\hat{O} = \hat{L}_\alpha = \sqrt{\Gamma_p}\hat{\sigma}_{ge}^{(\alpha)}$ with decay rate Γ_p. Here, $\hat{\sigma}_{bb'}^{(\alpha)} = [|b\rangle\langle b'|]_\alpha$ is acting on the αth background atom only. In (1) we neglect motion for the moment, thus $\hat{\rho} = \sum_{nm,\mathbf{b},\mathbf{b}'} \rho_{nm,\mathbf{b},\mathbf{b}'} |\pi_n; \mathbf{b}\rangle\langle\pi_m; \mathbf{b}'|$, where n and m label the electronic states of the Rydberg atoms and vector $\mathbf{b}$ labels the background atoms with each entry in $b_\alpha \in \{g, e, u\}$. Since (1) is intractable for many atoms, we now discuss three steps towards a simplified effective description.

Step 1. We assume the background gas settles into a steady state, enabling the interaction-enhanced imaging of states and positions of Rydberg atoms [29,30]. Its Hamiltonian for optical transitions is

$$\hat{H}_{\rm EIT} = \frac{\Omega_p}{2}\hat{\sigma}_{eg}^{(\alpha)} + \frac{\Omega_c}{2}\hat{\sigma}_{ue}^{(\alpha)} + \text{H.c.} - \Delta_p\hat{\sigma}_{ee}^{(\alpha)} - (\Delta_p + \Delta_c)\hat{\sigma}_{uu}^{(\alpha)}, \tag{2}$$

where Ω_p (Ω_c) and Δ_p (Δ_c) are probe (coupling) laser Rabi frequencies and detunings, respectively. Without interactions with Rydberg atoms, the background gas would be transparent for the probe beam due to (Rydberg) EIT for $\Omega_c \gg \Omega_p$, $\Delta_p = \Delta_c = 0$ [21–28].

The van der Waals interactions between the background and Rydberg atoms change this, and are described by

$$\hat{H}_{\rm int} = \sum_{a\in\{s,p\},\alpha n} V_{\alpha n}^{(ua)}(\mathbf{X}_n, \mathbf{x}_\alpha)\hat{\sigma}_{uu}^{(\alpha)}\hat{\sigma}_{aa}^{(n)}, \tag{3}$$

where $V_{\alpha n}^{(ua)}(\mathbf{X}_n, \mathbf{x}_\alpha) = C_{\eta(a),ua}/|\mathbf{X}_n - \mathbf{x}_\alpha|^\eta$, with $a \in \{s, p\}$ and $\eta(s) = 6$, $\eta(p) = 4$. For background atoms closer than a critical distance $d_{c,a} = (C_{\eta(a),ua}\Gamma_p/\Omega_c^2)^{1/\eta(a)}$ [31] with $a \in \{s, p\}$ to a Rydberg atom, interactions break EIT, resulting in an absorption shadow governed by $V_{\alpha n}^{(ua)}$, providing an indirect measurement of the position (and state) of the Rydberg atom through the center of the shadow (and its radius), as shown in Fig. 1. This is encoded in the steady-state optical susceptibility

$$\chi_p(t) = \Gamma_p/\Omega_p \,\mathrm{Im}\big[\hat{\rho}\sigma_{ge}^{(\alpha)}(t)\big], \tag{4}$$

describing absorption of the probe [29–31]. The interactions between background atoms are negligible [31,32] due to the small probability for two of them to be simultaneously excited to $|u\rangle$.

Step 2. We now add dipole-dipole interactions of the Rydberg atoms, with the Hamiltonian

$$\hat{H}_{\rm dd} = \sum_{n\neq m} W_{nm}(R_{nm})|\pi_n\rangle\langle\pi_m|, \tag{5}$$

for $W_{nm}(R) = C_3/R^3$, $R_{nm} = |\mathbf{X}_n - \mathbf{X}_m|$, and strength C_3. The complete Hamiltonian is thus $\hat{H} = \hat{H}_{\rm dd} + \hat{H}_{\rm EIT} + \hat{H}_{\rm int}$, which enters (1) along with $\hat{L}_\alpha$ to describe the dynamics of $\hat{\rho}$.

Now we reduce the Hilbert space dimension by adiabatically eliminating the states $|e\rangle$ and $|u\rangle$ [33] to work with a reduced density matrix $\hat{\rho}^{(\rm red)} = \sum_{nm}\rho_{nm}|\pi_n\rangle\langle\pi_m|$ for the Rydberg atoms alone. If the background gas reaches its steady state faster than the dipole-dipole transitions, $W_{nm} \ll \Gamma_p$, the latter are ignored during the elimination. For slightly larger dipolar interactions $W_{nm} \approx \Gamma_p$ relevant here, we nonperturbatively include them [33]. Either approach provides an effective equation

$$\dot{\hat{\rho}}^{(\rm red)} = -i[\hat{H}_{\rm eff} + \hat{H}_{\rm dd}, \hat{\rho}^{(\rm red)}] + \sum_\alpha \mathcal{L}_{\hat{L}_{\rm eff}^{(\alpha)}}[\hat{\rho}^{(\rm red)}], \tag{6}$$

in the Rydberg Hilbert space with effective operators $\hat{H}_{\rm eff} = \sum_{m,n,\alpha} h_{\rm eff}^{nm(\alpha)}(\mathbf{X}, \mathbf{x}_\alpha)|\pi_n\rangle\langle\pi_m|$ and $\hat{L}_{\rm eff}^{(\alpha)} = \sum_{m,n}\ell_{\rm eff}^{nm(\alpha)}(\mathbf{X}, \mathbf{x}_\alpha)|\pi_n\rangle\langle\pi_m|$.

For the next step we shall write (6) as $\dot{\hat{\rho}}^{(\rm red)} = \mathcal{A}[\hat{\rho}^{(\rm red)}]$, defining $\mathcal{A}$ as the superoperator acting on the reduced density matrix, which depends on $\hat{H}_{\rm dd}$, $\hat{H}_{\rm eff}$, and $\hat{L}_{\rm eff}$.

Step 3. We finally incorporate the motion of the Rydberg atoms, at positions $\mathbf{X}$ [34], extending the reduced density matrix to

$$\hat{\rho}^{(\rm red)} = \sum_{nm}\int d\mathbf{X}d\mathbf{X}'\rho(\mathbf{X}, \mathbf{X}')_{nm}|\mathbf{X}, \pi_n\rangle\langle\mathbf{X}', \pi_m|, \tag{7}$$

with $|\mathbf{X}, \pi_n\rangle \equiv |\mathbf{X}\rangle \otimes |\pi_n\rangle$, and changing $|\pi_n\rangle\langle\pi_m| \to |\mathbf{X}, \pi_n\rangle\langle\mathbf{X}, \pi_m|$ in (6). The effective motional master equation obtained from (6) is

$$\dot{\rho}(\mathbf{X}, \mathbf{X}')_{nm} = -\frac{i}{\hbar}\Bigg[-\frac{\hbar^2}{2M}\big(\nabla_{\mathbf{X}}^2 - \nabla_{\mathbf{X}'}^2\big)\rho(\mathbf{X}, \mathbf{X}')_{nm} + \sum_{kl}\mathcal{A}(\mathbf{X}, \mathbf{X}')_{kl}^{nm}\rho(\mathbf{X}, \mathbf{X}')_{kl}\Bigg], \tag{8}$$

with $\mathcal{A}(\mathbf{X}, \mathbf{X}')_{kl}^{nm} = E(\mathbf{X}, \mathbf{X}')_{kl}^{nm} + \Delta E(\mathbf{X}, \mathbf{X}')_{kl}^{nm} + i\gamma(\mathbf{X}, \mathbf{X}')_{kl}^{nm}$. Here, $E(\mathbf{X}, \mathbf{X}')_{kl}^{nm}$ involves dipole-dipole interactions $W_{nm}(\mathbf{X})$ and $\Delta E(\mathbf{X}, \mathbf{X}')_{kl}^{nm}$ background gas effects from $h_{\rm eff}^{nm(\alpha)}(\mathbf{X}, \mathbf{x}_\alpha)$. The terms arise from the unitary part of (6), with operators projected onto coordinates $\mathbf{X}$ ($\mathbf{X}'$) if they act from the left (right) on the density matrix. Similarly, $\gamma(\mathbf{X}, \mathbf{X}')_{kl}^{nm}$ accounts for the Lindblad part of (6) that depends on $\ell_{\rm eff}^{nm(\alpha)}(\mathbf{X}, \mathbf{x}_\alpha)$. We discuss the role of each element in $\mathcal{A}(\mathbf{X}, \mathbf{X}')$ for dynamics in detail later. To reach (8), we assume that the motion is even slower than the timescale of dipole-dipole transitions.

Square dephasing well. We shall now demonstrate a square well due to measurement-induced dephasing instead of a conservative potential. As an example, consider one Rydberg atom in the state $|s\rangle \equiv |80s\rangle$ with a lifetime $\tau \approx 620\ \mu$s at $T = 0$ K [35]. EIT-based position detection using $|u\rangle \equiv |31s\rangle$ is made spatially dependent by positioning all background

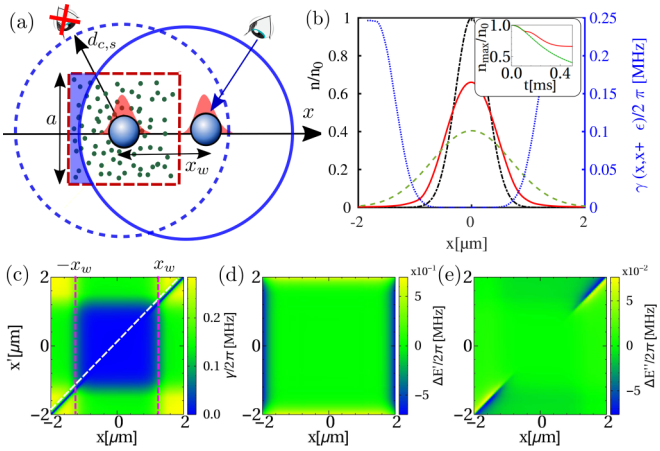

FIG. 2. Trapping a single particle through dephasing. (a) Sketch of an atom trapped in a dephasing well resulting from position measurements from the interrogating medium (green dots). (b) Probability density $n(x) = \rho(x, x)$ of the trapped particle at the initial time $t = 0$ with $\sigma = 0.4$ μm (black dotted-dashed line), and $t = 500$ μs later, in free space using $\gamma = 0$ (green dashed) or within the dephasing well (red line). The blue dotted line shows the one-dimensional (1D) cut $\gamma(x, x + \epsilon)$ near the diagonal, shown by the white dashed line in (c), for an offset $\epsilon = 0.15$ μm. Time evolution of the peak intensity is shown in the inset of (b). (c)–(e) Underlying dephasing rate $\gamma(x, x')$, and energy disorder $\Delta E'(x, x')$ and $\Delta E''(x, x')$ represented by (11) and (12), respectively [36]. x_w at the red dashed line indicates the size of the well, also sketched in (a).

atoms in a cubic volume $V = a^3$ as sketched in Fig. 2(a). We chose the side length a to be significantly smaller than the radius $d_{c,s}$ of the absorption shadow near the Rydberg atom [31], creating a *dephasing-free* region of width $2x_w$, with $x_w = d_{c,s} - a/2$, within which the optical signal gives no information on the Rydberg position, but records if the atom leaves that region.

For one Rydberg atom, $\hat{H}_{\rm dd} = 0$ in (6). We set $\mathbf{X} = [x, 0, 0]^T$, constraining the single Rydberg atom to one dimension for simplicity, while background atoms are distributed in three dimensions (3D), with positions $\mathbf{x}_\alpha$. The effective Hamiltonian $\hat{H}_{\rm eff} = h_{\rm eff}(x)|x\rangle\langle x|$ and Lindblad operator $\hat{L}^{(\alpha)}_{\rm eff} = \ell^{(\alpha)}_{\rm eff}(x, \mathbf{x}_\alpha)|x\rangle\langle x|$ enter (6) with [31]

$$h_{\rm eff}(x) = \sum_\alpha \frac{\Omega_p^2 \tilde{\Omega}_c^2 \tilde{V}(x, \mathbf{x}_\alpha)}{\tilde{\Omega}_c^4 + 4\tilde{V}^2(x, \mathbf{x}_\alpha)\left(|\tilde{\Gamma}_p|^2 - 4\Delta_p^2\right)}, \quad (9a)$$

$$\ell^{(\alpha)}_{\rm eff}(x, \mathbf{x}_\alpha) = \frac{2i\tilde{V}(x, \mathbf{x}_\alpha)\sqrt{\Gamma_p}\Omega_p}{2\tilde{V}(x, \mathbf{x}_\alpha)\tilde{\Gamma}_p - i\Omega_c^2}, \quad (9b)$$

where $\tilde{\Omega}_c^2 = \Omega_c^2 + 4\tilde{V}(x, \mathbf{x}_\alpha)\Delta_p$, $\tilde{\Gamma}_p = \Gamma_p - 2i\Delta_p$, and $\tilde{V}(x, \mathbf{x}_\alpha) = V_\alpha^{(us)}(\mathbf{X}, \mathbf{x}_\alpha) - \Delta_p - \Delta_c$. To focus on effects from dephasing only, without a net potential, we compensate $h_{\rm eff}(x)$ by a suitable external potential $V_{\rm ext}(x)$, chosen such that $h_{\rm eff}(x) + V_{\rm ext}(x) \approx 0$ [see Supplemental Material (SM) [36]]. Using these in (8), we find the motional master equation for the single Rydberg atom of mass M in a dephasing well as

$$\dot{\rho}(x, x') = -\frac{i}{\hbar}\left[-\frac{\hbar^2}{2M}\left(\nabla_x^2 - \nabla_{x'}^2\right)\rho(x, x')\right] + [i\Delta E(x, x')/\hbar - \gamma(x, x')/2]\rho(x, x'), \quad (10)$$

with

$$\gamma(x, x') = \sum_\alpha \left|\ell^{(\alpha)}_{\rm eff}(x, \mathbf{x}_\alpha)\right|^2 + \left|\ell^{(\alpha)}_{\rm eff}(x', \mathbf{x}_\alpha)\right|^2 - 2\,{\rm Re}\left[\ell^{(\alpha)}_{\rm eff}(x, \mathbf{x}_\alpha)\ell^{(\alpha)*}_{\rm eff}(x', \mathbf{x}_\alpha)\right], \quad (11)$$

$$\Delta E(x, x') = \Delta E'(x, x') + \Delta E''(x, x'), \quad (12)$$

where $\Delta E'(x, x') = \tilde{h}_{\rm eff}(x) - \tilde{h}_{\rm eff}(x')$ and $\Delta E''(x, x') = \sum_\alpha {\rm Im}[\ell^{(\alpha)}_{\rm eff}(x, \mathbf{x}_\alpha)\ell^{(\alpha)*}_{\rm eff}(x', \mathbf{x}_\alpha)]$, shown in Figs. 2(c)–2(e) with $\tilde{h}_{\rm eff}(x) = h_{\rm eff}(x) + V_{\rm ext}(x)$. Equation (9b) depends on the EIT parameters and interactions, which can both be tuned. Together with the spatial background atom distribution, this allowed creating a dephasing well shown in Fig. 2(c). We see in the $\gamma(x, x')$ profile that dephasing will affect coherences $\rho(x, x')$ for x inside and x' outside the decoherence-free region, or vice versa.

We initialize the Rydberg atom in a wave packet $\psi(x) = \exp[-(x - x_0)^2/(2\sigma^2)]/(\pi\sigma^2)^{1/4}$ centered in the dephasing well [see the black dotted-dashed line in Fig. 2(b)]. In free space, the wave packet would diffuse on timescales of interest. In the background gas, evolving the effective Lindblad master equation (10) using the high-level language XMDS [37,38], for parameters given in the SM [36], we show the time-evolving density in Fig. 2(b).

We can see that spreading is strongly suppressed (red) due to the square dephasing well (blue dotted), compared to the case without dephasing $\gamma = 0$ (green dashed). This could be observed by high-precision Rydberg atom location measurements [30,39]. The dephasing inhibits any further diffusion of the wave function beyond a critical time $t_c \approx 300$ μs, shown in the inset of Fig. 2(b). This suppression is not due to a conservative potential, since the disorder from the background $h_{\rm eff}(x)$ has been canceled. Trapping arises instead solely due to the dephasing of coherences between different spatial locations $x \neq x'$. In this sense, it is decoherence due to the position measurement itself that provides the confinement in the well. Similar ideas in another context were explored in Refs. [12,40], for which we propose here an experimental platform using realistic parameters. The energy of the trapped atom is conserved since the environment only causes dephasing.

Separation-dependent dimer decoherence. In order to extend the above to binding, we require the dephasing strength to depend on the *relative* coordinate in a dimer instead of absolute coordinates. This feature is naturally provided because the EIT-based Rydberg state measurements cease to be effective for very short dimer separations, for reasons discussed now. The dimer atoms are constrained to Rydberg states $|s\rangle \equiv |43s\rangle$ and $|p\rangle \equiv |43p\rangle$, with a lifetime of 42 and 62.5 μs, respectively, at $T = 300$ K [35]. The dimer can then be in states $|\pi_1\rangle = |ps\rangle$ and $|\pi_2\rangle = |sp\rangle$ with a resultant lifetime of 25 μs. The background gas Rydberg state is $|u\rangle \equiv |38s\rangle$.

Now, we implement step 2 discussed earlier to derive the set of effective operators $\hat{H}_{\rm eff}$ and $\hat{L}_{\rm eff}$ discussed in (6) for a Rydberg dimer ($N = 2$). The effective model developed in Ref. [31] is not valid for close dimer separations, hence we extended it here. To keep the problem tractable, we take the relative coordinate r of the dimer atoms as the only motional degree of freedom, fixing their positions in terms of

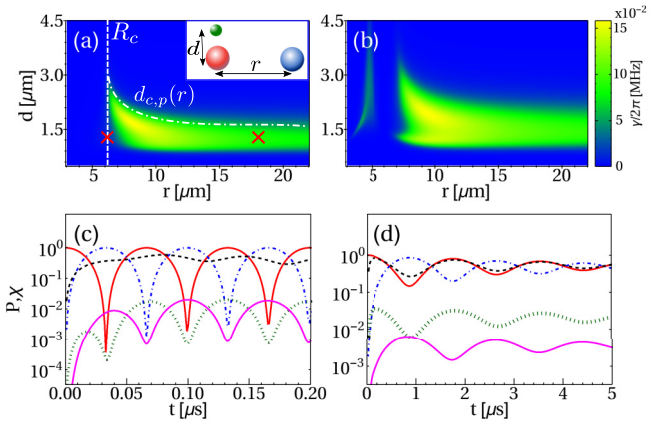

FIG. 3. Dimer decoherence ceases at close distances. (a), (b) Variation of dephasing rate $\gamma(r, d)$ in a Rydberg dimer probed by a single detector atom, (a) using the three-body master equation Eq. (1) and (b) using the effective model Eq. (6). Parameters are in Ref. [41]. The geometry is shown in the inset. (c) Population of $|gps\rangle$ (red solid), $|gsp\rangle$ (blue dotted-dashed), $|eps\rangle$ (green dotted), $|esp\rangle$ (magenta solid), and optical susceptibility as described by Eq. (4) $\chi = \kappa\,\mathrm{Im}[\langle g|\hat{\rho}|e\rangle]$ (black-dashed line) [41] for $r = 6\ \mu$m and $d = 1.05\ \mu$m. (d) Same as (c) but for $r = 18\ \mu$m. Both configurations are marked with red crosses in (a).

$\bar{\mathbf{X}}_{1,2} = \mathbf{R}_0 \mp r\mathbf{e}_x/2$, where $\mathbf{R}_0$ is the center of mass of dimer atoms and $\mathbf{e}_x$ a unit vector along the x axis. Equation (6) in the relative coordinate r contains $\hat{H}_{\mathrm{eff}} = \sum_{n,m,\alpha} h_{\mathrm{eff}}^{nm(\alpha)}(r, \mathbf{x}_\alpha)|\pi_n\rangle\langle\pi_m|$ and $\hat{L}_{\mathrm{eff}} = \sum_{n,m,\alpha} \ell_{\mathrm{eff}}^{nm(\alpha)}(r, \mathbf{x}_\alpha)|\pi_n\rangle\langle\pi_m|$, which we derive in the SM [36]. The closed forms of $h_{\mathrm{eff}}^{nm(\alpha)}(r, \mathbf{x}_\alpha)$ and $\ell_{\mathrm{eff}}^{nm(\alpha)}(r, \mathbf{x}_\alpha)$ are long and technical, and are inserted into our code using the export feature of *Mathematica*. To validate the derivation and demonstrate the cessation of decoherence for close-proximity dimer atoms, we compare results from Eqs. (1) and (6), using a test case with a Rydberg dimer flanked by a single background atom as shown in the inset of Fig. 3(a), which also defines the coordinates r and d.

For Figs. 3(a) and 3(b), the dimer is initialized in $(|\pi_1\rangle + |\pi_2\rangle)/\sqrt{2}$, which is evolved in time, neglecting motion, according to Eqs. (1) and (6). For all parameters, we can fit $\langle\pi_1|\hat{\rho}|\pi_2\rangle$ by the exponential $\exp[-\gamma(r, d)t]$, from which we show the decay rate γ in the figure. There are two main features: (i) As discussed in Ref. [31], the background atom only decoheres the dimer if placed at a distance $d_{c,s}(1.3\ \mu\mathrm{m}) < d < d_{c,p}(2\ \mu\mathrm{m})$ from the latter. (ii) This decoherence ceases for dimer separations below $R_c \approx 6\ \mu$m, where we empirically find $R_c \propto C_3^{1/3}$. Here, the background can no longer adiabatically follow dipole-dipole interactions, as demonstrated in Figs. 3(c) and 3(d). These show the essential state populations together with the optical susceptibility χ_p (black dashed line) of the background atom, defined in (4), when the dimer is initialized in $|\pi_1\rangle$, the population of which is shown as a red solid line. The background atom should show nonzero susceptibility only for dimer state $|\pi_1\rangle$, if it can adiabatically follow state changes. However, the susceptibility is synchronized with the linear population oscillations only at large separation. For small r, the background atom can thus no longer "measure" the state of the dimer, and decoherence ceases.

This creates a well in the relative coordinate r, based on dephasing. A dimer with an initially close separation, moving towards larger distances due to constituent repulsion, will encounter an abrupt dephasing barrier in its relative coordinate. From this key result, we will show that the barrier can be strong enough to cause binding of the dimer. From Fig. 3(b), it can be seen that the effective model qualitatively captures all the features correctly, if we manually remove the decoherence feature at $r \approx 5\ \mu$m, done in the following to tackle simulations in a background gas with $N_{\mathrm{bg}} \approx 2000$.

Binding by dephasing. We now consider the motion of the dimer atoms, as in step 3, in the regime of strong dipolar interactions, using the improved effective model benchmarked in Fig. 3. The relative coordinate r of the dimer atoms is the only motional degrees of freedom, restricted along the x axis. Hence, the dynamic position $\mathbf{X}$ in $\hat{\rho}^{(\mathrm{red})}$ in (7) is now replaced by the relative coordinate r of the Rydberg dimer. When deriving the master equation as in (8), $h_{\mathrm{eff}}^{nm(\alpha)}(r, \mathbf{x}_\alpha)$ and $l_{\mathrm{eff}}^{nm(\alpha)}(r, \mathbf{x}_\alpha)$ are projected onto coordinates $r(r')$ if they act from the left (right) on the density matrix. We find

$$\begin{aligned}\dot{\rho}(r, r')_{nm} = &-\frac{i}{\hbar}\Bigg[-\frac{\hbar^2}{2\mu}\left(\nabla_r^2 - \nabla_{r'}^2\right)\rho(r, r')_{nm} \\ &+ \sum_k \left[W_{nk}(r)\rho(r, r')_{km} - W_{km}(r')\rho(r, r')_{nk}\right]\Bigg] \\ &+ \sum_{k,l}\left(i\frac{\Delta E(r, r')_{kl}^{nm}}{\hbar} - \gamma(r, r')_{kl}^{nm}\right)\rho(r, r')_{kl},\end{aligned} \tag{13}$$

where $\mu = M/2$ is the reduced mass of the dimer atoms, $W_{12} = W_{21}$ are dipole-dipole interactions (5), and $W_{nn} = 0$. The background gas enters through an energy detuning $\Delta E(r, r')_{kl}^{nm}$ and dephasing $\gamma(r, r')_{kl}^{nm}$ given as

$$\Delta E(r, r')_{kl}^{nm} = \sum_\alpha \left[h_{\mathrm{eff}}^{nk(\alpha)}(r, \mathbf{x}_\alpha)\delta_{l,m} - h_{\mathrm{eff}}^{lm(\alpha)}(r', \mathbf{x}_\alpha)\delta_{n,k}\right] + \mathrm{Im}\left[\mathcal{O}(r, r')_{kl}^{nm}\right], \tag{14a}$$

$$\gamma(r, r')_{kl}^{nm} = \mathrm{Re}\left[\mathcal{O}(r, r')_{kl}^{nm}\right], \tag{14b}$$

$$\begin{aligned}\mathcal{O}(r, r')_{kl}^{nm} = \sum_\alpha \Bigg[&\left[\ell_{\mathrm{eff}}^{nk(\alpha)}(r, \mathbf{x}_\alpha)\right]^* \ell_{\mathrm{eff}}^{lm(\alpha)}(r', \mathbf{x}_\alpha) \\ &- \frac{1}{2}\sum_j \Big[\left[\ell_{\mathrm{eff}}^{nj(\alpha)}(r, \mathbf{x}_\alpha)\right]^* \ell_{\mathrm{eff}}^{jk(\alpha)}(r, \mathbf{x}_\alpha)\delta_{l,m} \\ &+ \left[\ell_{\mathrm{eff}}^{lj(\alpha)}(r', \mathbf{x}_\alpha)\right]^* \ell_{\mathrm{eff}}^{jm(\alpha)}(r', \mathbf{x}_\alpha)\delta_{n,k}\Big]\Bigg].\end{aligned} \tag{14c}$$

The first two lines of (13) describe unitary quantum dynamics from dipole-dipole interactions. We can diagonalize the corresponding Hamiltonian (5) at separation r as in $\hat{H}_{\mathrm{dd}}(r)|\varphi_k\rangle = U_k(r)|\varphi_k\rangle$ to find two Born-Oppenheimer surfaces, one repulsive and one attractive: $U(r)_{\mathrm{rep/att}} = \pm C_3/r^3$ [20]. The underlying eigenstates (molecular states) are $|\varphi_{\mathrm{rep/att}}\rangle = (|\pi_1\rangle \pm |\pi_2\rangle)/\sqrt{2}$.

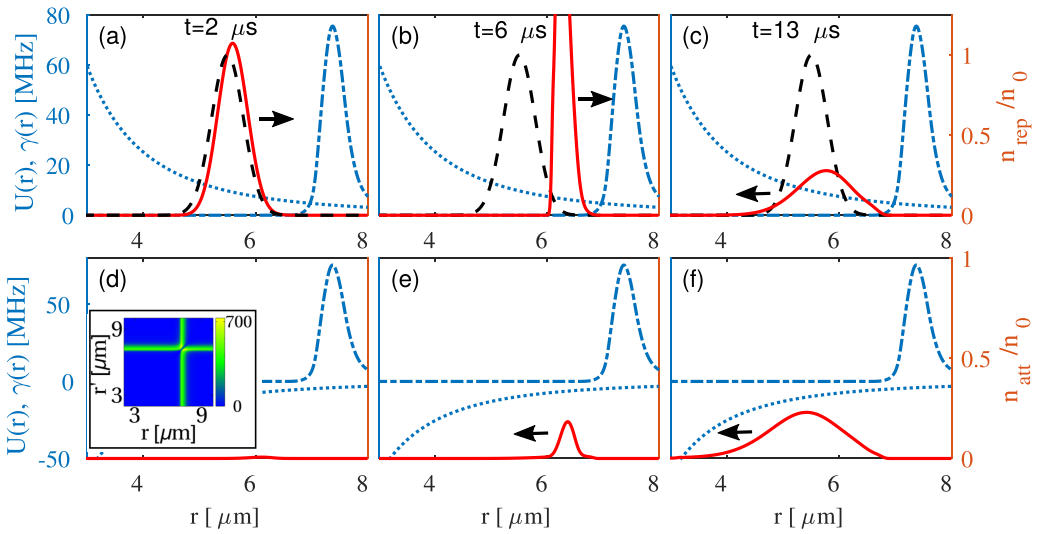

FIG. 4. Dimer bound in a *repulsive* potential due to reflection of a dephasing barrier. The dimer atoms are initially separated by $r = 5.5\ \mu$m with $\sigma = 0.4\ \mu$m and immersed in a background gas of density $\rho_{\rm bg} = 1.6 \times 10^{21}\ {\rm m}^{-3}$. (a)–(c) [(d)–(f)] Normalized probability density $n_{\rm rep}/n_0$ [$n_{\rm att}/n_0$] (solid red line) on the repulsive [attractive] surfaces (dotted blue line) at times $t = 2$, 6, and 13 μs. Here, n_0 is the initial peak density. We also show the initial densities at $t = 0$ (black dashed line) and the dephasing rate $\gamma(r, r)^{12}_{12}$ (blue dotted-dashed line) and $\gamma(r, r')^{nn}_{nn}$, defined in (14b), in the inset of (d). Arrows indicate the direction of motion of wave packets. See Supplemental Material for a movie.

$\Delta E(r, r')^{nm}_{kl}$ represents energy shifts due to the background atoms. Here, this disorder is negligible compared to the dipolar interactions. The terms $\gamma(r, r')^{nm}_{kl}$ contain all central decoherence features. For us, two terms dominate, spatial decoherence between distances r and r' through $\gamma(r, r')^{nn}_{nn}$ [see the inset in Fig. 4(d)] and decoherence between electronic states $|\pi_1\rangle$ and $|\pi_2\rangle$ $\gamma(r, r')^{12}_{12}$, nearly indistinguishable on the scale of the inset except for a diagonal contribution $\gamma(r, r)^{12}_{12}$ shown as a blue dotted-dashed line in the main panels. At small separations ($r < R_c \approx 7.5\ \mu$m here), decoherence ceases since the background gas can no longer infer the dimer state. At r just above R_c, decoherence is maximal, since for larger r the critical radius $d_{c,p}(r)$ becomes smaller, reducing the volume of background atoms that contribute.

We initialize the dimer in the repulsive electronic state with a Gaussian relative wave function $\hat{\rho}(t = 0) = |\phi_0\rangle|\varphi_{\rm rep}\rangle\langle\varphi_{\rm rep}|\langle\phi_0|$, with $\langle r|\phi_0\rangle = \phi_0(r) = \exp[-(r - r_0)^2/(2\sigma^2)]/(\pi\sigma^2)^{1/4}$. From this initial state, we numerically solve (13). As shown in Fig. 4, the Rydberg dimer on the repulsive surface reaches the dephasing barrier $\gamma(r)$ at a larger dimer separation r and reflects from it with a probability $\rho_{\rm rep} \approx 47\%$ to subsequently climb the repulsive potential $U(r)$ again. The reflected part of the dimer wave packet continues to oscillate on the repulsive energy surface, forming a decoherence-induced metastable bound state. Without binding by dephasing, the wave packet would reach $r > 10\ \mu$m by time $t = 13\ \mu$s and the dimer would dissociate. Besides the reflected component on the repulsive surface, we see in Fig. 4(f) a comparable fraction incoherently coupled to the attractive surface [34]. $\rho_{\rm rep}$ can be experimentally controlled by varying the strength of the dephasing barrier through EIT parameters. The binding on the repulsive surface could be seen in an experiment at, e.g., $t = 20\ \mu$s, when the population on the attractive surface would have collided and ionized, while the reflected wave packet on the repulsive surface reached its inner turning point instead of dissociation. The separation dependence of $\gamma(r)$ is set through a competition between the dipole-dipole interaction and medium response timescales, and does not require any spatially selective optics. While there is some minor dissipation in the scenario of Fig. 4, it plays no role in the binding process, as we have verified with a simulation without the terms in (13) that cause it. We confirmed that the dynamics in Fig. 4 is nearly unchanged if $\Delta E(r, r')^{nm}_{kl}$ and the components of $\gamma(r, r')^{nm}_{kl}$ not discussed above are neglected, but show figures of all of these in the SM [36].

Conclusions and outlook. We have shown how two central features of nature, trapped states and bound states, can arise solely based on dephasing spatial or electronic quantum coherence. Dephasing can be controlled through measurements of absolute or relative coordinates.

This significantly extends earlier reports of binding by particle loss [7,10,14–19], generalizing them to the most widespread type of decoherence and removing the need for dissipation. We discussed both features with examples that should be within reach of state-of-the-art experiments, in which a Rydberg atom is embedded in a cold EIT medium, and the position and electronic states of the former can be controllably decohered by the latter [29–31,34,42]. Ultimately, binding or trapping through dephasing may give rise to new states of quantum matter, similar to the dissipative stabilization of a Mott insulator [43], but removing the need to compensate loss.

Acknowledgments. We gladly acknowledge interesting discussions with S. Rammohan, A. Sreedharan, S. Tiwari, and S. Whitlock, and thank the Max-Planck society for financial support under the MPG-IISER partner group program as well as the Indo-French Centre for the Promotion of Advanced Research - CEFIPRA. K.M. acknowledges the Ministry of Education for support from the Prime Minister's Research Fellowship (PMRF).

[1] B. H. Bransden and C. J. Joachain, *Physics of Atoms and Molecules* (Pearson Education, New York, 2003).

[2] M. A. Schlosshauer, *Decoherence and the Quantum-to-Classical Transition* (Springer, Berlin, 2007).

[3] M. Schlosshauer, Rev. Mod. Phys. **76**, 1267 (2005).

[4] D. Suter and G. A. Álvarez, Rev. Mod. Phys. **88**, 041001 (2016).

[5] J. F. Poyatos, J. I. Cirac, and P. Zoller, Phys. Rev. Lett. **77**, 4728 (1996).

[6] F. Verstraete, M. M. Wolf, and J. I. Cirac, Nat. Phys. **5**, 633 (2009).

[7] S. L. Vuglar, D. V. Zhdanov, R. Cabrera, T. Seideman, C. Jarzynski, and D. I. Bondar, Phys. Rev. Lett. **120**, 230404 (2018).

[8] B. Misra and E. C. G. Sudarshan, J. Math. Phys. **18**, 756 (1977).

[9] A. G. Kofman and G. Kurizki, Nature (London) **405**, 546 (2000).

[10] B. Zhu, B. Gadway, M. Foss-Feig, J. Schachenmayer, M. L. Wall, K. R. A. Hazzard, B. Yan, S. A. Moses, J. P. Covey, D. S. Jin, J. Ye, M. Holland, and A. M. Rey, Phys. Rev. Lett. **112**, 070404 (2014).

[11] B. Yan, S. A. Moses, B. Gadway, J. P. Covey, K. R. A. Hazzard, A. M. Rey, D. S. Jin, and J. Ye, Nature (London) **501**, 521 (2013).

[12] J. B. Mackrory, K. Jacobs, and D. A. Steck, New J. Phys. **12**, 113023 (2010).

[13] G. Gordon, I. E. Mazets, and G. Kurizki, Phys. Rev. A **87**, 052141 (2013).

[14] M. Lemeshko and H. Weimer, Nat. Commun. **4**, 2230 (2013).

[15] J. J. García-Ripoll, S. Dürr, N. Syassen, D. M. Bauer, M. Lettner, G. Rempe, and J. I. Cirac, New J. Phys. **11**, 013053 (2009).

[16] N. Syassen, D. M. Bauer, M. Lettner, T. Volz, D. Dietze, J. J. Garcia-Ripoll, J. I. Cirac, G. Rempe, and S. Dürr, Science **320**, 1329 (2008).

[17] C. Ates, B. Olmos, W. Li, and I. Lesanovsky, Phys. Rev. Lett. **109**, 233003 (2012).

[18] B. Cui, S. Hou, W. Wang, and X. X. Yi, J. Phys. B: At., Mol. Opt. Phys. **47**, 215303 (2014).

[19] A. J. Daley, J. M. Taylor, S. Diehl, M. Baranov, and P. Zoller, Phys. Rev. Lett. **102**, 040402 (2009).

[20] S. Wüster and J. M. Rost, J. Phys. B: At., Mol. Opt. Phys. **51**, 032001 (2018).

[21] M. Fleischhauer, A. Imamoglu, and J. P. Marangos, Rev. Mod. Phys. **77**, 633 (2005).

[22] I. Friedler, D. Petrosyan, M. Fleischhauer, and G. Kurizki, Phys. Rev. A **72**, 043803 (2005).

[23] A. K. Mohapatra, T. R. Jackson, and C. S. Adams, Phys. Rev. Lett. **98**, 113003 (2007).

[24] S. Mauger, J. Millen, and M. P. A. Jones, J. Phys. B: At., Mol. Opt. Phys. **40**, F319 (2007).

[25] A. K. Mohapatra, M. G. Bason, B. Butscher, K. J. Weatherill, and C. S. Adams, Nat. Phys. **4**, 890 (2008).

[26] H. Schempp, G. Günter, C. S. Hofmann, C. Giese, S. D. Saliba, B. D. DePaola, T. Amthor, M. Weidemüller, S. Sevinçli, and T. Pohl, Phys. Rev. Lett. **104**, 173602 (2010).

[27] S. Sevinçli, C. Ates, T. Pohl, H. Schempp, C. S. Hofmann, G. Günter, T. Amthor, M. Weidemüller, J. D. Pritchard, D. Maxwell, A. Gauguet, K. J. Weatherill, M. P. A. Jones, and C. S. Adams, J. Phys. B: At., Mol. Opt. Phys. **44**, 184018 (2011).

[28] V. Parigi, E. Bimbard, J. Stanojevic, A. J. Hilliard, F. Nogrette, R. Tualle-Brouri, A. Ourjoumtsev, and P. Grangier, Phys. Rev. Lett. **109**, 233602 (2012).

[29] G. Günter, M. Robert-de-Saint-Vincent, H. Schempp, C. S. Hofmann, S. Whitlock, and M. Weidemüller, Phys. Rev. Lett. **108**, 013002 (2012).

[30] G. Günter, H. Schempp, M. Robert-de Saint-Vincent, V. Gavryusev, S. Helmrich, C. Hofmann, S. Whitlock, and M. Weidemüller, Science **342**, 954 (2013).

[31] D. W. Schönleber, A. Eisfeld, M. Genkin, S. Whitlock, and S. Wüster, Phys. Rev. Lett. **114**, 123005 (2015).

[32] B. Olmos, W. Li, S. Hofferberth, and I. Lesanovsky, Phys. Rev. A **84**, 041607(R) (2011).

[33] F. Reiter and A. S. Sørensen, Phys. Rev. A **85**, 032111 (2012).

[34] S. Wüster, Phys. Rev. Lett. **119**, 013001 (2017).

[35] I. I. Beterov, I. I. Ryabtsev, D. B. Tretyakov, and V. M. Entin, Phys. Rev. A **79**, 052504 (2009).

[36] See Supplemental Material at http://link.aps.org/supplemental/10.1103/PhysRevA.105.L041102 for the derivation of an effective model in the regime of relatively strong dipolar interactions and the construction of a dephasing well.

[37] G. R. Dennis, J. J. Hope, and M. T. Johnsson, Comput. Phys. Comm. **184**, 201 (2013).

[38] G. R. Dennis, J. J. Hope, and M. T. Johnsson, http://www.xmds.org/ (2012).

[39] N. Thaicharoen, A. Schwarzkopf, and G. Raithel, Phys. Rev. A **92**, 040701(R) (2015).

[40] P. Facchi, S. Pascazio, A. Scardicchio, and L. S. Schulman, Phys. Rev. A **65**, 012108 (2001).

[41] Rydberg states: $|s\rangle = |43s\rangle$, $|p\rangle = |43p\rangle$ for the aggregate atoms and $|r\rangle = |38s\rangle$ for the detector atom with parameteres $\Omega_p/2\pi = 1.3$ MHz, $\Omega_c/2\pi = 30$ MHz, $\Gamma_p/2\pi = 6.1$ MHz, $\Delta_p = \Delta_c = 0$ MHz, $C_3/2\pi = 1619$ MHz μm^3, $C_{6,s}/2\pi = -87$ MHz μm^6, $C_{4,p}/2\pi = -1032$ MHz μm^4, and $\kappa = \Gamma_p/\Omega_p$.

[42] H. Schempp, G. Günter, S. Wüster, M. Weidemüller, and S. Whitlock, Phys. Rev. Lett. **115**, 093002 (2015).

[43] R. Ma, B. Saxberg, C. Owens, N. Leung, Y. Lu, J. Simon, and D. I. Schuster, Nature (London) **566**, 51 (2019).